ATOMIC-SCALE STUDY OF THE SUPERCONDUCTING PROXIMITY EFFECT IN MANGANITE/CUPRATE THIN-FILM HETEROSTRUCTURES

Hao Zhang[1], Igor Fridman[1], Nicolas Gauquelin[2], Gianluigi Botton[2], John Y.T. Wei[1, 3]

[1]*Department of Physics, University of Toronto, Toronto ON, M5S1A7, Canada*
[2]*Canadian Centre for Electron Microscopy, McMaster University, Hamilton ON, L8S4M1 Canada*
[3]*Canadian Institute for Advanced Research, Toronto ON, M5G1Z8, Canada*

ABSTRACT

Superconducting proximity effects that are extremely long-ranged have recently been reported in manganite/cuprate thin-film heterostructures, and attributed to spin-triplet correlations involving odd-frequency pairing. To probe this novel scenario microscopically, we studied *c*-axis multilayer $La_{2/3}Ca_{1/3}MnO_3/YBa_2Cu_3O_{7-\delta}$ (LCMO/YBCO) thin films using scanning tunneling spectroscopy (STS), scanning transmission electron microscopy (STEM), x-ray diffraction (XRD) and electrical transport. STS measurements of bilayers at 4.2 K showed no proximity-induced pairing gap on the ferromagnetic LCMO overlayer down to 5 nm thickness. Cross-sectional STEM revealed double CuO-chain intergrowths in the YBCO layer that form regions with the so-called 247 lattice structure. These nanoscale 247 regions do not show up in XRD, but can physically account for the reduction of superconducting critical temperature (T_c) vs. YBCO thickness in LCMO/YBCO multilayers. As further corroboration, we observed similar T_c reduction in $LaNiO_3$/YBCO multilayers, where $LaNiO_3$ is not ferromagnetic. These results suggest that microstructural defects, rather than the ferromagnetism, are responsible for the long-ranged attenuation of superconductivity reported in *c*-axis LCMO/YBCO heterostructures.

INTRODUCTION

In recent years, there have been numerous studies of the interplay between ferromagnetism and superconductivity in heteroepitaxial thin films comprising the ferromagnetic manganites and superconducting cuprates.[1-7] An observation of particular interest is the dependence of the superconducting critical temperature (T_c) on the *c*-axis layer thicknesses in $La_{2/3}Ca_{1/3}MnO_3/YBa_2Cu_3O_{7-\delta}$ (LCMO/YBCO) multilayers.[8,9] The length scale of this dependence has been attributed to extremely long-ranged superconducting proximity effect

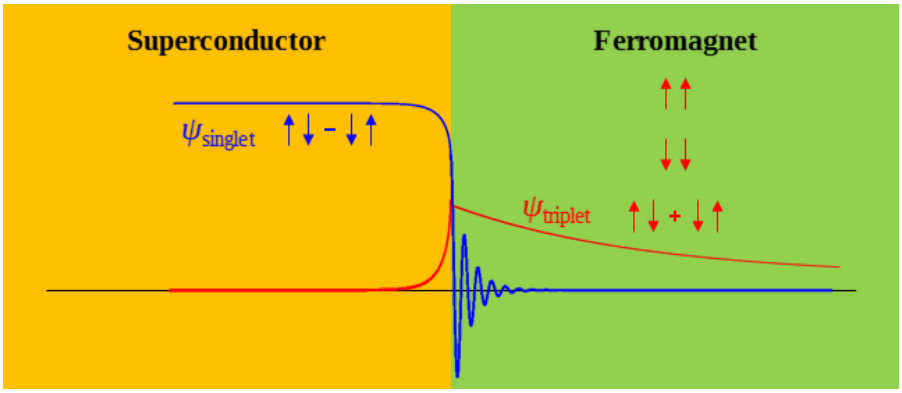

Figure 1: Schematic illustration of long-ranged proximity effect across a superconductor/ ferromagnet junction. Odd-frequency spin-triplet pairs with even-parity orbital symmetry are induced near the interface and penetrate into the ferromagnet far deeper than spin-singlet pairs, since spin-triplet pairs are not easily broken by the exchange field in the ferromagnet.

associated with spin-triplet pair formation.[6,10-25] A schematic illustration of this effect is shown in Figure 1. Unlike spin-singlet pairs, spin-triplet pairs are not easily broken by an exchange field, and can thus penetrate deep into the ferromagnet. Theoretical models based on odd-frequency pairing have been proposed, to reconcile the triplet pairing with *d*-wave orbital symmetry, which is known to predominate in YBCO.[26,27] However, other interfacial mechanisms such as charge transfer,[28-30] orbital reconstruction,[31] spin diffusion[9] and induced magnetic modulation[32,33] are also believed to affect the superconductivity in LCMO/YBCO heterostructures.

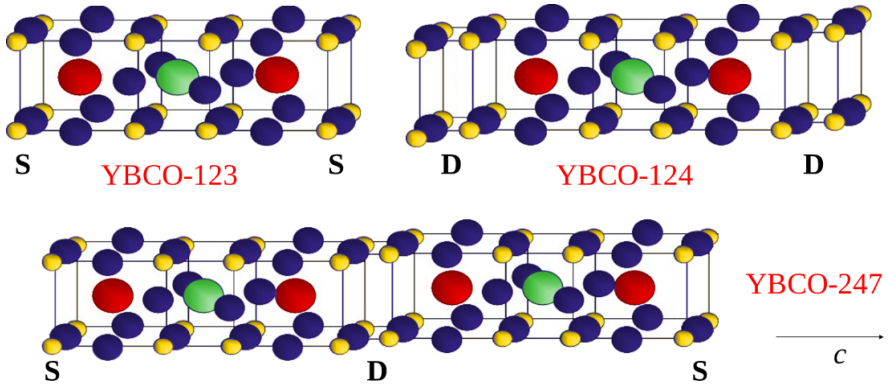

Figure 2: The lattice structures of YBCO-123, YBCO-124 and YBCO-247, with the Cu, Y, and Ba atoms color-labeled as yellow, green, and red, respectively. The CuO chain sites are labelled as S and D for single-chains and double-chains respectively.

Despite these prior studies, direct microscopic evidence for long-ranged proximity effect in *c*-axis manganite/cuprate heterostructures has been lacking. In this paper, we report on an atomic-scale study of the phenomenon using scanning tunneling spectroscopy (STS) and scanning transmission electron microscopy (STEM), and correlate the results with macroscopic measurements including x-ray diffraction (XRD) and electrical transport. First, STS can be used to directly probe proximity effects in ferromagnet-on-superconductor bilayers, by measuring the quasiparticle density of states (DOS) on the top layer.[34-36] A gap in the DOS spectrum would be a distinct signature of proximity-induced pair potential, whose dependence on top-layer thickness could give a measure of the proximity length scale.[37] Second, a crucial aspect of LCMO/YBCO heterostructures that has not been well studied is the microscopic stoichiometry of the YBCO layer. The Y-Ba-Cu-O compounds are exceptional among the cuprates in having CuO chains, the number of which per unit cell allows the cation stoichiometry to vary between the so-called YBCO-123, YBCO-124 and YBCO-247 phases (see Figure 2).[38,39] Since these phases differ in their optimal T_c,[40-45] microscopic variations in the YBCO stoichiometry of LCMO/YBCO heterostructures could affect the resistively-measured T_c and thus the physical interpretation.

EXPERIMENTAL

The *c*-axis LCMO/YBCO multilayer and YBCO unilayer films used in our study were epitaxially grown on (001)-oriented (La,Sr)(Al,Ta)O_3 (LSAT) and $SrTiO_3$ (STO) substrates using pulsed laser-ablated deposition (PLD). Multilayer films comprising $LaNiO_3$ (LNO) and YBCO, where LNO is paramagnetic, were also grown for comparison. Our PLD system is equipped with a 248 nm KrF excimer laser, and the deposition was done with a repetition rate of 2-5 Hz and fluence of ~2 J/cm^2 at 700°-800°C in 200-500 mTorr of O_2. Following deposition, the films were annealed in-situ by slow cooling from the growth temperature to 300°C in 45 minutes in 760 Torr of O_2 to fully oxygenate the YBCO layer. In our films, the LCMO layer ranged from 5 to 25 nm, the YBCO layer from 10 to 50 nm, while the LNO layer was 25 nm in thickness.[46]

The STS measurements were made with a home-built scanning tunneling microscope operating at 4.2 K in ~1 mTorr of ^{4}He exchange gas. Pt-Ir tips were used, and the typical junction impedance was ~10 GΩ. The conductance *dI/dV* spectra were obtained from numerically differentiating the average of 50 *I-V* curves at each tip location. The spectra were measured on several samples for each layer thickness, and at multiple locations on each sample to ensure reproducibility.[47]

The cross-sectional STEM images were taken using a FEI Titan 80–300 microscope fitted with a high-brightness field emission gun and CEOS aberration correctors for both condenser and objective lens aberrations. The microscope operated at 200 keV in scanning mode using the high-angle annular dark-field (HAADF) imaging method, which is sensitive to the atomic number contrast. The elemental identification made by the HAADF imaging was corroborated by atomic-scale electron energy loss spectroscopy (EELS).[48]

The XRD patterns were taken using θ - 2θ method with Cu K_a radiation from a Philips PW2273/20 X-ray tube. Finally, electrical resistance of the films was measured using standard AC lock-in technique in the four-contact configuration, in which silver contacts were sputtered onto the surface of the films in parallel strips. Temperature dependence of the resistance was recorded using a variable-temperature dipper probe inside a liquid helium dewar, and the sample temperature was monitored with a Cernox sensor to 0.1 K accuracy.

RESULTS AND DISCUSSION

The STS data taken on bilayer LCMO/YBCO films grown on STO substrates are shown in Figure 3. Figure 3(a) shows the *dI/dV* spectra for three films, ranging from 10 nm to 20 nm of LCMO deposited over 20 nm of YBCO. The plotted spectra have been normalized by their values at 50 mV for comparison. These spectra have a characteristic V shape with some asymmetry, as well as substantial conductance at zero bias indicating finite DOS at the Fermi level. No clear gap structure is seen, in contrast to data taken on a unilayer YBCO film as shown

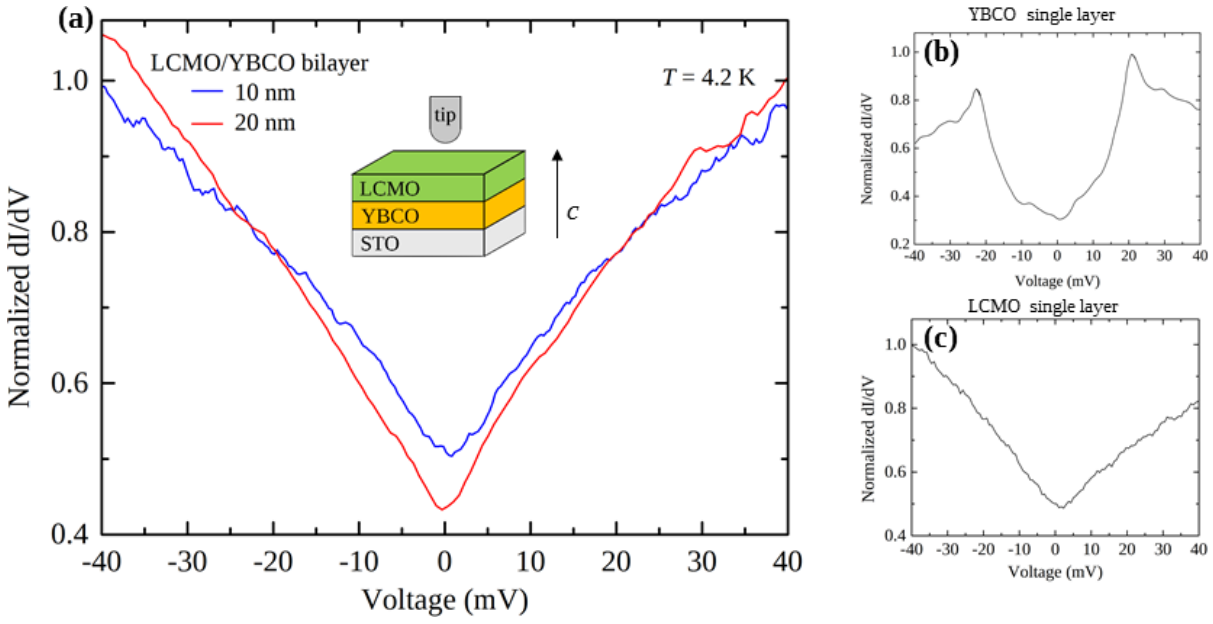

Figure 3: Scanning tunneling conductance spectra measured with a Pt-Ir tip on thin-film samples at 4.2 K. Panel (a) shows spectra taken on bilayer LCMO/YBCO films, for 10-nm (blue curve) and 20-nm (red curve) LCMO thickness. These spectra are distinct from data taken on a unilayer YBCO film (b), but similar to data taken on a unilayer LCMO film (c).

in Figure 3(b). The bilayer spectra data are also qualitatively similar to data taken on a unilayer LCMO film as shown in Figure 3(c). Similar V-shaped spectra have been seen in other transition-metal oxides, and appear to be characteristic of strongly-correlated oxide materials.[3,49] When the LCMO layer is reduced to 5 nm, the *dI/dV* spectra (not shown) are also V-shaped similar to unilayer LCMO films. Thus, down to 5 nm of LCMO thickness, there is no clear spectral signature of superconducting proximity effect in *c*-axis LCMO/YBCO bilayers. These observations are consistent with conventional short-ranged proximity effect associated with strong suppression of spin-singlet pairing in the nearly half-metallic LCMO layer.[44]

Figure 4 shows a high-resolution HAADF-STEM image taken over the cross section of a 25-nm/50-nm bilayer LCMO/YBCO film grown on LSAT substrate. The color labels indicate different elements as identified from the HAADF-STEM images, with the Cu, Y, and Ba atoms color-labeled as yellow, green, and red, respectively. To the right of the LCMO/YBCO interface (dotted blue line), there are three unit cells of YBCO-123 characterized by single CuO chains between Ba atoms, followed by a unit cell of YBCO-124 characterized by double CuO chains between Ba atoms. This alternation of single and double CuO chains forms a unit cell of YBCO-247, which is essentially a superlattice of YBCO-123 and YBCO-124 blocks. Further on the right of Figure 4 is another YBCO-247 unit cell, also containing both a single and a double CuO chain. Between the two YBCO-247 unit cells, a unit cell of YBCO with missing CuO chain is seen, in which two adjacent Ba layers join together with no CuO chain in between. Such chain-less region can be explained in terms of compensation for the double CuO chains in the YBCO-247 regions, as the YBCO target used for PLD had 123 stoichiometry.

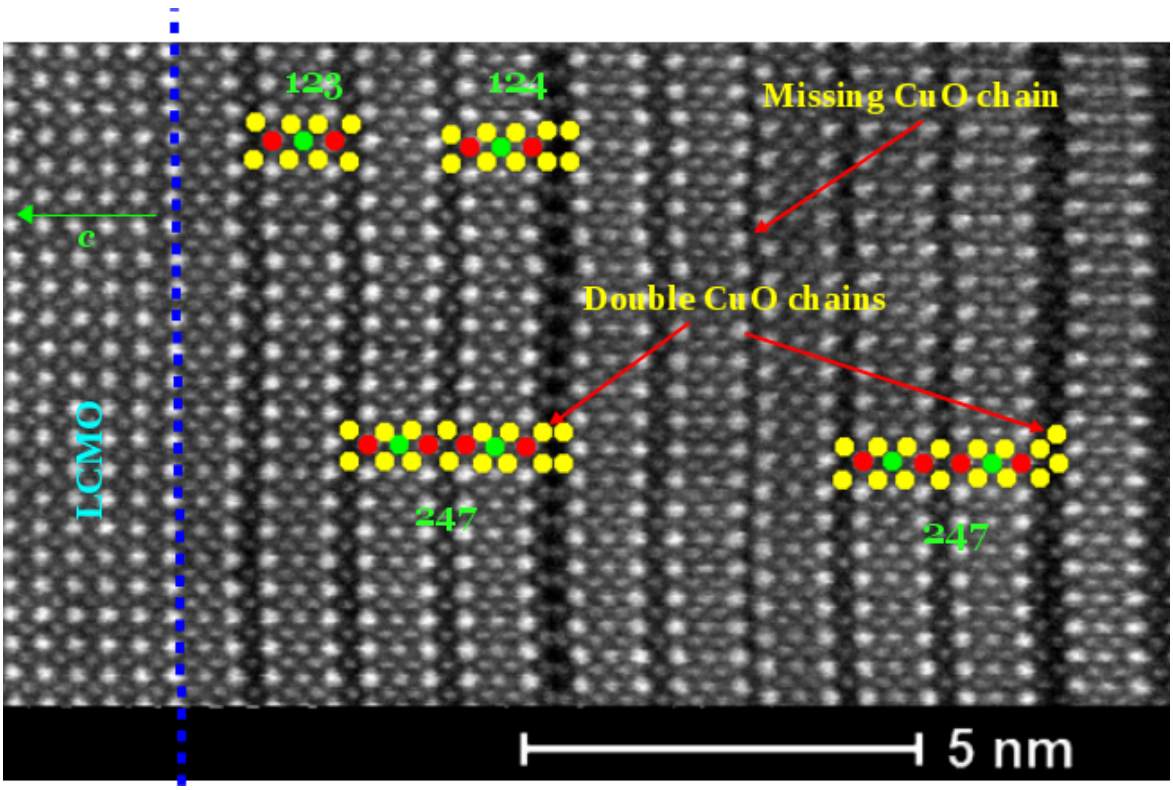

Figure 4: High-resolution HAADF-STEM image of a 25-nm/50-nm bilayer LCMO/YBCO film grown on (001)-oriented LSAT substrate. Blue dotted line indicates the LCMO/YBCO interface, and the Cu, Y, and Ba atoms are respectively color-labeled as yellow, green and red. While the YBCO layer nominally has 123 stoichiometry, the intergrowths of double-CuO chains effectively form nanoscale YBCO-247 regions.

To examine the pervasiveness of the nanoscale YBCO-247 intergrowths, we compare the STEM images of a bilayer LCMO/YBCO and of a unilayer YBCO. In the bilayer LCMO/YBCO film shown in Figure 5(a), YBCO-247 regions appear throughout the YBCO layer, with the double-CuO chains indicated by the arrows. In contrast, these double-CuO intergrowths are mostly absent in unilayer YBCO films grown under similar conditions, as shown in Figure 5(b). Interestingly, the nanoscale YBCO-247 intergrowths that appear in the high-resolution STEM image of a bilayer LCMO/YBCO film do not appear in its XRD pattern. In fact, the locations of the diffraction peaks for the bilayer LCMO/YBCO film (Figure 5c) and for a unilayer YBCO film (Figure 5d) are indistinguishable. All the major peaks are identified in terms of either YBCO-123, LCMO or LSAT, although the peaks for LCMO and LSAT cannot be distinguished because of their close lattice parameters. For the bilayer case, by relating the YBCO (005)- and (007)-peaks with $2\theta = 38.55°$ and $2\theta = 55.06°$ respectively, we find the *c*-axis lattice parameter in the YBCO layer to be 11.68 Å, in agreement with fully oxygenated YBCO-123.[50] It should be emphasized that no peaks associated with YBCO-247 are visible in the XRD data for either the bilayer or unilayer film, within the resolution of our instrument.

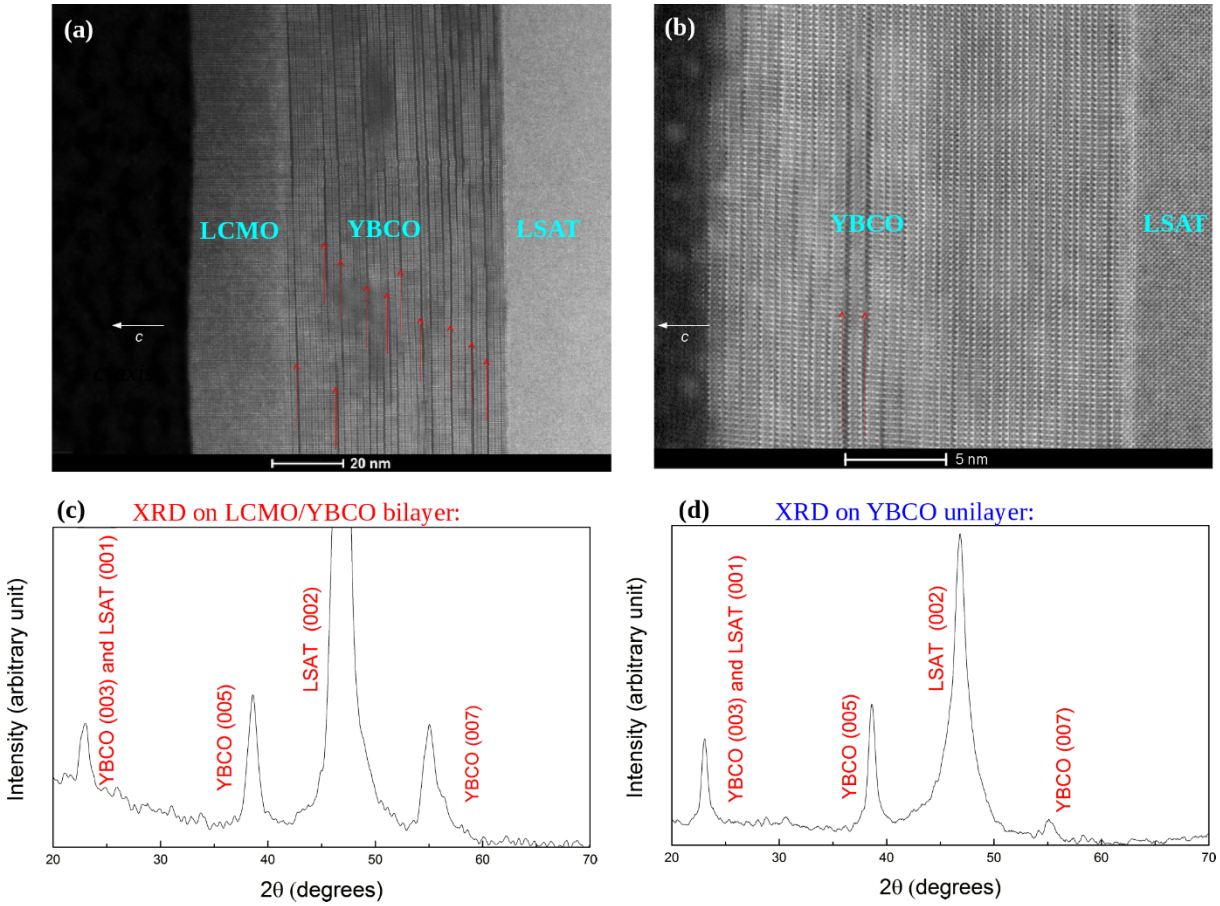

Figure 5: Comparison between bilayer LCMO/YBCO and unilayer YBCO films. Panel (a) shows the STEM image of a bilayer film: nanoscale YBCO-247 regions appear throughout the YBCO layer, with the double-CuO chains indicated by arrows. These double-CuO intergrowths are largely absent in a unilayer YBCO film, as shown in panel (b). The peak locations in the XRD patterns for the bilayer film (panel c) and for the unilayer film (panel d) are indistinguishable. Note that the nanoscale YBCO-247 regions appearing in the bilayer film do not appear in the XRD data within the resolution of our instrument.

The resistively-measured T_c in our bilayer LCMO/YBCO films is evidently affected by the presence of nanoscale YBCO-247 regions. Figure 6 plots the resistance R vs. temperature T data taken on various films. Each R-vs.-T curve is normalized to its R value at room temperature to facilitate comparison. The unilayer YBCO films grown on LSAT or STO substrates show sharp superconducting transitions with T_c near 90 K, consistent with fully-oxygenated YBCO-123. These results indicate that the resistive T_c of the YBCO layer is largely insensitive to its lattice mismatch with the substrate material, at least down to 25-nm YBCO thickness. However, the 25-nm/25-nm bilayer LCMO/YBCO film shows a much lower and broader T_c, near 60 K, than any of the unilayer YBCO films, indicating that the addition of an epitaxial LCMO overlayer significantly reduces the resistive T_c in the YBCO layer. We can plausibly attribute this T_c reduction to the nanoscale YBCO-247 regions seen in our high-resolution STEM images, since YBCO-247 has generally shown lower T_c than either YBCO-124 or fully-oxygenated YBCO-123 according to bulk studies.[51,52] We note that pure YBCO-123 samples can also show reduced T_c when under-oxygenated, with $T_c \sim 60$ K corresponding to $\delta \sim 0.5$ or $YBa_2Cu_3O_{6.5}$.[53] However, this alternative scenario of under-oxygenation is not likely to explain our R-vs.-T data, since the LCMO overlayer was grown in-situ at an even higher oxygen pressure than the YBCO layer, and the entire bilayer was given ample time to fully oxygenate during in-situ post-annealing in 760 Torr of oxygen.

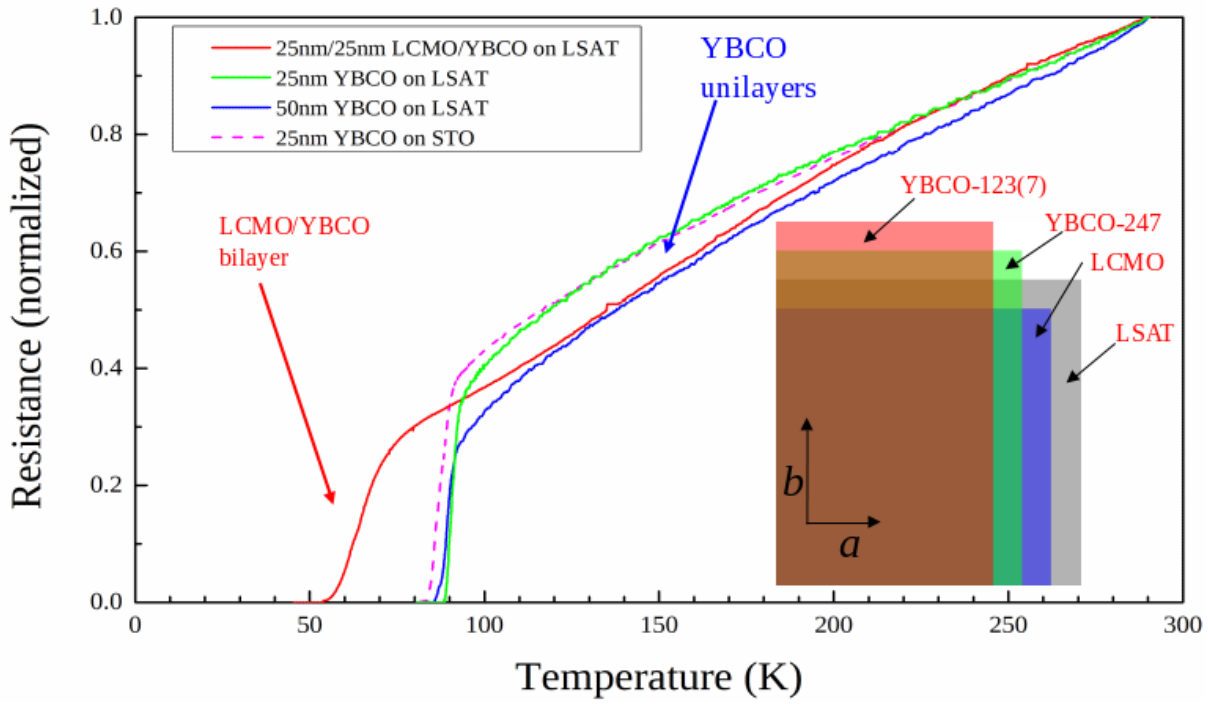

Figure 6: Plot of normalized resistance vs. temperature for unilayer YBCO and bilayer LCMO/YBCO films. All the unilayer films show sharp superconducting transitions with T_c near 90 K. The 25-nm/25-nm bilayer LCMO/YBCO film shows a broadened and reduced T_c near 60 K. The inset shows a schematic diagram illustrating the differences in both lattice symmetry and lattice parameters of the *ab*-plane lattice structure between YBCO-123, YBCO-247, LCMO, and LSAT. In the diagram, the relative length scales between the *a*- and *b*-axes for each material, and between the materials, are exaggerated for clarity.

To explain the formation of the nanoscale YBCO-247 regions in our LCMO/YBCO films and the absence of these intergrowths in unilayer YBCO films, we examine the lattice structures of the materials involved in the heteroepitaxy. It is well known that all the superconducting phases of Y-Ba-Cu-O are orthorhombic due to the CuO chain that runs along the *b*-axis. YBCO-247 is less orthorhombic than YBCO-123, because of its shorter *b*-axis due to the inter-chain attraction within the double-CuO chains. As shown in the schematic diagram of the *ab*-plane lattice structures of YBCO-123, YBCO-247, LCMO, and LSAT in the inset of Figure 6, since both the LCMO overlayer and the LSAT substrate have cubic lattices, their combined mismatch in lattice symmetry with the YBCO layer favors the formation of the less orthorhombic YBCO-247 phase. In addition to this lattice-symmetry mismatch, the *a*- and *b*-axes lattice parameters of both LCMO and LSAT are closer to YBCO-247 than to YBCO-123. Thus the lattice-parameter mismatch, from both sides of the YBCO layer, also favors the formation of YBCO-247. In the YBCO layer, the conversion to YBCO-247 via the intergrowth of double CuO chains provides an effective mechanism for relieving the heteroepitaxial strain imposed by both the LCMO overlayer and LSAT substrate.

To examine the role played by ferromagnetism in the T_c reduction of LCMO/YBCO heterostructures and to further corroborate our microstructural interpretation of T_c reduction, we also grew LNO/YBCO heterostructures and measured their R vs. T for comparison. LNO is a paramagnetic perovskites with similar lattice parameters (within ~ 0.26%) as LCMO. Thus the

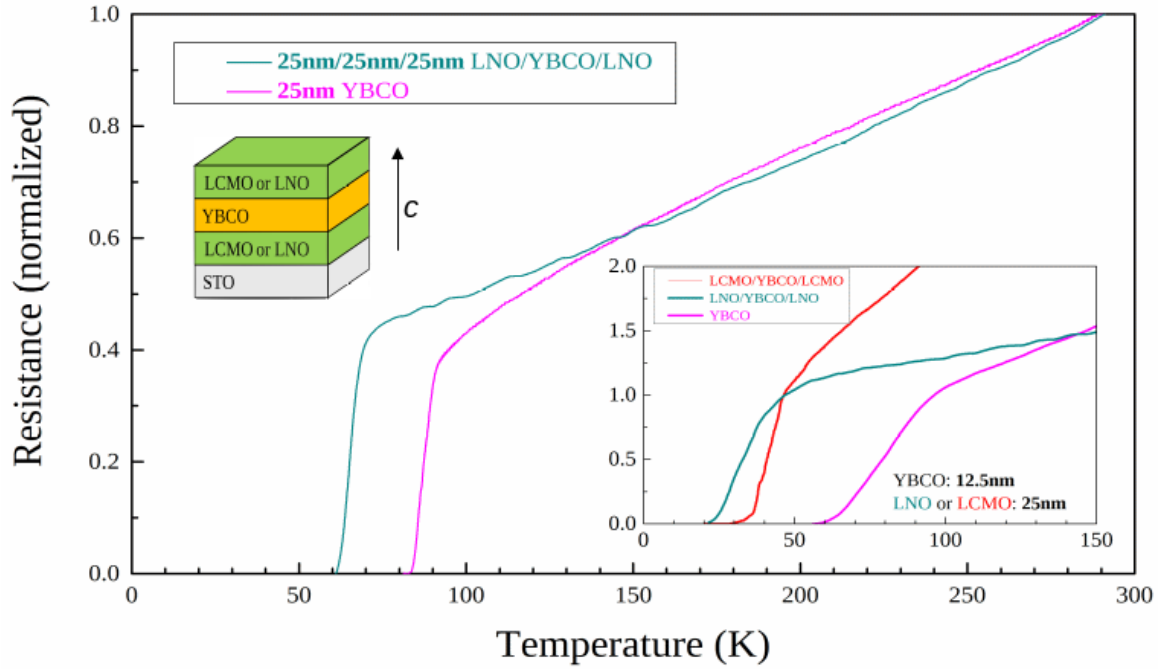

Figure 7: Plot of normalized resistance vs. temperature for trilayer LNO/YBCO/LNO and unilayer YBCO films grown on (001)-oriented STO substrates. In the trilayer, YBCO is sandwiched between two LNO layers, each 25 nm thick, to symmetrize the strain. At 25 nm YBCO thickness, the trilayer film shows a T_c ~ 60 K, which is much lower than that of the unilayer YBCO film. The inset shows similar behavior at 12.5 nm YBCO thickness, with data from trilayer LCMO/YBCO/LCMO included for comparison: superconductivity onsets at a much lower temperature (~ 45 K), for both LNO/YBCO/LNO and LCMO/YBCO/LCMO, as compared with unilayer YBCO.

YBCO layer in LNO/YBCO heterostructures is subject to similar heteroepitaxial strain as but without the ferromagnetism in LCMO/YBCO heterostructures. Figure 7 compares the *R*-vs.-*T* plots between trilayer LNO/YBCO/LNO and unilayer YBCO films. All the samples were grown on (001)-oriented STO substrates. For the trilayer films, the YBCO layer was sandwiched between two LNO layers, each 25 nm thick, to symmetrize the strain from both the top and the bottom sides. When the YBCO layer is 25 nm thick, the LNO/YBCO/LNO film has a $T_c \sim 60$ K, which is much lower than a unilayer YBCO film but close in value to a LCMO/YBCO/LCMO film with the same YBCO thickness. The inset of Figure 7 shows a comparison of the *R*-vs.-*T* data for LNO/YBCO/LNO, LCMO/YBCO/LCMO and unilayer YBCO, with the YBCO layer thickness fixed at 12.5 nm. Here the trilayer films also show much lower T_c than the unilayer film. In particular, the onset of superconductivity for LNO/YBCO/LNO occurs at a similarly low temperature (~ 45 K) as LCMO/YBCO/LCMO. Since LNO is not ferromagnetic, the similar dependence of T_c on YBCO layer thickness, between the LNO/YBCO and LCMO/YBCO heterostructures, indicates that the ferromagnetism plays a negligible role in the T_c reduction seen in the latter.

CONCLUSION

In summary, we have carried out an atomic-scale study of the superconducting proximity effect in *c*-axis LCMO/YBCO heterostructures. STS, STEM, XRD and *R*-vs.-*T* measurements were performed on bilayer LCMO/YBCO and unilayer YBCO thin films, grown epitaxially on either LSAT or STO substrates by PLD. The STS measurements at 4.2 K on bilayer LCMO/YBCO films observed no proximity-induced pairing gaps down to 5-nm LCMO thickness. The HAADF-STEM images taken on the bilayer films revealed nanoscale YBCO-247 regions characterized by double CuO-chain intergrowths, which are largely absent in the unilayer YBCO films and can be attributed to heteroepitaxial lattice mismatch of the YBCO layer with both the LCMO overlayer and LSAT substrate. These nanoscale 247 regions do not appear in XRD, but can physically explain the lower resistive T_c measured in LCMO/YBCO multilayers. As further corroboration, we observed similar T_c reduction in LNO/YBCO multilayers, where LNO is not ferromagnetic. These results suggest that the anomalously long-ranged attenuation of superconductivity reported in *c*-axis LCMO/YBCO thin-film heterostructures is more likely due to strain-induced microstructural defects than to the ferromagnetism.

ACKNOWLEDGEMENTS

Work supported by NSERC, CFI-OIT and the Canadian Institute for Advanced Research.

REFERENCES

[1] V. A. Vas'ko, V. A. Larkin, P. A. Kraus, K. R. Nikolaev, D. E. Grupp, C. A. Nordman, and A. M. Goldman, Phys. Rev. Lett. 78, 1134 (1997).
[2] P. Kraus, A. Bhattacharya, and A. M. Goldman, Phys. Rev. B 64, 220505(R) (2001).
[3] Z. Y. Chen, A. Biswas, I. Zutić, T. Wu, S. B. Ogale, R. L. Greene, and T. Venkatesan, Phys. Rev. B 63, 212508 (2001).
[4] Z. Sefrioui, D. Arias, V. Pena, J. E. Villegas, M. Varela, P. Prieto, C. Leon, J. L. Martinez, and J. Santamaria, Phys. Rev. B 67, 214511(2003).
[5] A. I. Buzdin, Rev. Mod. Phys. 77, 935 (2005).
[6] K. Dybko, K. Werner-Malento, P. Aleshkevych, M. Wojcik, M. Sawicki, and P. Przyslupski, Phys. Rev. B 80, 144504 (2009).
[7] For recent studies, see C. Visani, Z. Sefrioui, J. Tornos, C. Leon, J. Briatico, M. Bibes, A. Barthelemy, J. Santamaria, and J. E. Villegas, Nat. Phys. 8, 539 (2012), and references therein.

[8] H.-U. Habermeier, G. Cristiani, R. K. Kremer, O. Lebedev, and G. van Tendeloo, Physica C 364, 298 (2001).
[9] V. Pena, C. Visani, J. Garcia-Barriocanal, D. Arias, Z. Sefrioui, C. Leon, and J. Santamaria, Phys. Rev. B 73, 104513 (2006).
[10] F. S. Bergeret, A. F. Volkov, and K. B. Efetov, Phys. Rev. Lett. 86, 4096 (2001).
[11] F. S. Bergeret, A. F. Volkov, and K. B. Efetov, Rev. Mod. Phys. 77, 1321 (2005).
[12] R. S. Keizer, S. T. B. Goennenwein, T. M. Klapwijk, G. Miao, G. Xiao and A. Gupta, Nature 439, 825 (2006).
[13] Y. Asano, Y. Tanaka, A. A. Golubov, and S. Kashiwaya, Phys. Rev. Lett. 99, 067005 (2007).
[14] Z. Ping Niu and D. Y. Xing, Phys. Rev. Lett. 98, 057005 (2007).
[15] Y. Kalcheim, T. Kirzhner, G. Koren, and O. Millo, Phys. Rev. B 83, 064510 (2011).
[16] A. S. Mel'nikov, A. V. Samokhvalov, S. M. Kuznetsova, and A. I. Buzdin, Phys. Rev. Lett. 109, 237006 (2012).
[17] F. S. Bergeret and I. V. Tokatly, Phys. Rev. Lett. 110, 117003 (2013).
[18] Roland Grein, Tomas Löfwander, and Matthias Eschrig, Phys. Rev. B 88, 054502 (2013).
[19] V. I. Zdravkov, J. Kehrle, G. Obermeier, D. Lenk, H.-A. Krug von Nidda, C. Müller, M. Yu. Kupriyanov, A. S. Sidorenko, S. Horn, R. Tidecks, and L. R. Tagirov Phys. Rev. B 87, 144507 (2013).
[20] T. Golod, A. Rydh, V. M. Krasnov, I. Marozau, M. A. Uribe-Laverde, D. K. Satapathy, Th. Wagner, and C. Bernhard, Phys. Rev. B 87, 134520 (2013).
[21] M. Egilmez, J. W. A. Robinson, Judith L. MacManus-Driscoll, L. Chen, H. Wang and M. G. Blamire, Europhys. Lett. 106, 37003 (2014).
[22] Yoav Kalcheim, Israel Felner, Oded Millo, Tal Kirzhner, Gad Koren, Angelo Di Bernardo, Mehmet Egilmez, Mark G. Blamire, and J. W. A. Robinson, Phys.Rev. B 89, 180506(R) (2014).
[23] A. Singh, S. Voltan, K. Lahabi, and J. Aarts, Phys. Rev. X 5, 021019 (2015).
[24] C. Visani, F. Cuellar, A. Pérez-Muñoz, Z. Sefrioui, C. León, J. Santamaría, and Javier E. Villegas, Phys. Rev. B 92, 014519 (2015).
[25] Ya. V. Fominov, Y. Tanaka, Y. Asano, and M. Eschrig, Phys. Rev. B 91, 144514 (2015).
[26] C. C. Tsuei and J. R. Kirtley, Rev. Mod. Phys. 72, 969 (2000).
[27] J. Y. T. Wei, N.-C. Yeh, D. F. Garrigus, and M. Strasik, Phys. Rev. Lett. 81, 2542 (1998).
[28] T. Holden, H.-U. Habermeier, G. Cristiani, A. Golnik, A. Boris, A. Pimenov, J. Humlicek, O. I. Lebedev, G. Van Tendeloo, B. Keimer, and C. Bernhard, Phys. Rev. B 69, 064505 (2004).
[29] M. Varela, A. R. Lupini, V. Pena, Z. Sefrioui, I. Arslan, N. D. Browning, J. Santamaria, and S. J. Pennycook, e-print arXiv:cond-mat/0508564 (2006).
[30] V. Pena, T. Gredig, J. Santamaria, and I. K. Schuller, Phys. Rev. Lett. 97, 177005 (2006).
[31] J. Chakhalian, J. W. Freeland, H.-U. Habermeier, G. Cristiani, G. Khaliullin, M. van Veenendaal, and B. Keimer, Science 318, 1114 (2007).
[32] J. Chakhalian, J. W. Freeland, G. Srajer, J. Strempfer, G. Khaliullin, J. C. Cezar, T. Charlton, R. Dalgliesh, C. Bernhard, G. Cristiani, H.-U. Habermeier, and B. Keimer, Nat. Phys. 2, 244 (2006).
[33] J. Stahn, J. Chakhalian, C. Niedermayer, J. Hoppler, T. Gutberlet, J. Voigt, F. Treubel, H.-U. Habermeier, G. Cristiani, B. Keimer, and C. Bernhard, Phys. Rev. B 71, 140509(R) (2005).
[34] L. Crétinon, A. K. Gupta, H. Sellier, F. Lefloch, M. Faure, A. Buzdin, and H. Courtois, Phys. Rev. B 72, 024511 (2005).
[35] I. Asulin, O. Yuli, G. Koren, and O. Millo, Phys. Rev. B 74, 092501 (2006).
[36] I. Asulin, O. Yuli, I. Felner, G. Koren, and O. Millo, Phys. Rev. B 76, 064507 (2007).
[37] P. C. van Son, H. van Kempen, and P. Wyder, Phys. Rev. Lett. 59, 2226 (1987).
[38] J. Karpinski, S. Rusiecki, B. Bucher, E. Kaldis, and E. Jilek, Physica C 161, 618 (1989).

[39] Donald E. Morris, Andrea G. Markelz, Boris Fayn, Janice H. Nickel, Physica C 168, 153 (1990).
[40] R. J. Cava, B. Batlogg, R. B. van Dover, D. W. Murphy, S. Sunshine, T. Siegrist, J. P. Remeika, E. A. Rietman, S. Zahurak, and G. P. Espinosa, Phys. Rev. Lett. 58, 1676 (1987).
[41] P. Bordet, C. Chaillout, J. Chenavas, J. L. Hodeau, M. Marezio, J. Karpinski, and E. Kaldis, Nature 334, 596 (1988).
[42] D. E. Morris, J. H. Nickel, J. Y. T. Wei, N. G. Asmar, J. S. Scott, U. M. Scheven, C. T. Hultgren, A. G. Markelz, J. E. Post, P. J. Heaney, D. R. Veblen, and R. M. Hazen, Phys. Rev. B 39, 7347 (1989).
[43] D. E. Morris, N. G. Asmar, J. Y. T. Wei, J. H. Nickel, R. L. Sid, J. S. Scott, and J. E. Post, Phys. Rev. B 40, 11406 (1989).
[44] J. Karpinski, E. Kaldis, S. Rusiecki, E. Jilek, P. Fischer, P. Bordet, C. Chaillout, J. Chenavas, J. L. Hodeau, and M. Marezio, Physica C 160, 449 (1989).
[45] J. L. Tallon, D. M. Pooke, R. G. Buckley, M. R. Presland, and F. J. Blunt, Phys. Rev. B 41, 7220 (1990).
[46] H. Zhang, N. Gauquelin, G. A. Botton, and J. Y. T. Wei, Appl. Phys. Lett. 103, 052606 (2013).
[47] I. Fridman, L. Gunawan, G. A. Botton, and J. Y. T. Wei, Phys. Rev. B 84, 104522 (2011).
[48] N. Gauquelin, G.-z. Zhu, H. Zhang, J. Y. T. Wei and G. A. Botton, manuscript in preparation.
[49] A. K. Raychaudhuri, K. P. Rajeev, H. Srikanth, and N. Gayathri, Phys. Rev. B 51, 7421 (1995).
[50] J. J. Capponi, C. Chaillout, A. W. Hewat, P. Lejay, M. Marezio, N. Nguyen, B. Raveau, J. L. Soubeyroux, J. L. Tholence, and R. Tournier, Europhys. Lett. 3, 1301 (1987).
[51] M. Kato, M. Nakanishi, T. Miyano, T. Shimizu, M. Kakihana, K. Yoshimura, and K. Kosuge, J. Solid State Chem. 139, 266 (1998).
[52] A. Irizawa, T. Ohmura, T. Shibata, M. Kato, K. Yoshimura, K. Kosuge, Y. Ito, H. Michor, and G. Hilscher, J. Phys. Soc. Jpn. 71, 574 (2002).
[53] Ruixing Liang, D. A. Bonn, and W. N. Hardy, Phys. Rev. B 73, 180505(R) (2006).